PROCEEDINGS A

royalsocietypublishing.org/journal/rspa

Research

Cite this article: Liguori P, Gei M. 2023 New actuation modes of composite dielectric elastomers. *Proc. R. Soc. A* **479**: 20230168. https://doi.org/10.1098/rspa.2023.0168

Received: 8 March 2023
Accepted: 7 June 2023

Subject Areas:
mechanics

Keywords:
dielectric elastomers, composite materials, electro-elasticity

Authors for correspondence:
Pietro Liguori
e-mail: liguorip@cardiff.ac.uk
Massimiliano Gei
e-mail: massimiliano.gei@dia.units.it

New actuation modes of composite dielectric elastomers

Pietro Liguori[1] and Massimiliano Gei[2]

[1]School of Engineering, Cardiff University, The Parade, Cardiff CF24 3AA, Wales, UK
[2]Department of Engineering and Architecture, University of Trieste, via A. Valerio 6/1, 34127 Trieste, Italy

MG, 0000-0003-3869-7504

The typical actuation mode of a dielectric elastomer membrane subjected to an electric field across its thickness is in-plane expansion. We show that, by selecting properly the contrast between phases (i.e. shear moduli and permittivity ratios), a hierarchical laminate may display longitudinal contraction when actuated in the same way. In particular, simple and second rank laminates are investigated. The latter performs in general better; however, we provide a guideline on how to optimize the microstructure to limit the values of the contrast parameters at which the new 'non-conventional' mode becomes available. As the requirements in terms of permittivity ratio of the two phases are somewhat extreme, we review the availability of materials that have been processed so far to assess the viability of such composite devices.

1. Introduction

Dielectric elastomer actuators consist of thin elastomer membranes actuated by a difference in electric potential across the thickness [1] which induces in-plane expansion at large strains. They have been exploited in several fields of engineering, ranging from soft robotics [2–4] to biomedical devices [5–7] to energy harvesters [8–10] (the review [11] provides an extended overview of the topic).

A method to improve the actuation performance is to create a composite material assembled by embedding a high-dielectric reinforcement in a much softer matrix [12–14]. In a series of papers, it has been shown that the most effective microstructure to achieve a specific performance at equal volume fraction of the component phases is that of hierarchical laminates [15–22].

THE ROYAL SOCIETY PUBLISHING

The goal of this paper is to investigate laminate hierarchical devices made up of soft dielectric elastomers which exhibit actuation modes that are different from the expected in-plane expansion. In particular, in our small-strain, plane-strain analysis, we focus on the conditions to reach the counterintuitive and 'unconventional' in-plane *contraction* actuation mode. A similar mode has been observed in devices devoted to electromechanical energy conversion; however, the mechanism exploited in that case is different than that highlighted here being associated with either transverse expansion due to reduction of voltage across the thickness or phase transition (see, e.g. [23,24]).

We show the possibility to accomplish contraction in both rank-one and rank-two laminates by carefully selecting their properties. We first examine the features of the former composite to achieve the new mode assuming two types of boundary conditions. Its availability is analysed to understand how each phase deforms. We then compare the features of the latter composite to the former to show how rank-two laminates are able to enhance this mode of actuation. As the number of parameters involved is larger, we provide a guideline on how to optimize them to obtain the desired actuation.

We conclude the paper assessing the viability of such composite devices with an appraisal of the available materials to be used in principle as a reinforcement in a laminate to achieve the required values of the contrast parameters to display contraction.

2. Plane-strain linear electro-elastic actuation of rank-one laminates

As pointed out in the Introduction, we deal with small-strain electro-elasticity. We consider first a rank-one layered composite elastomer slab which is obtained by repeating a unit cell consisting of two compressible dielectric materials as shown in figure 1*a*. The soft matrix material is denoted by '*a*' whereas the stiffer phase is indicated with '*b*'; the lamination angle for the simply layered materials is θ_1. The composite is defined by the volume fraction of each phase, c^a and c^b, respectively, subjected to the constraint $c^a + c^b = 1$. The—perfect—interface between the two materials is singled out by normal and tangential unit vectors, namely $\boldsymbol{n}^0$ and $\boldsymbol{m}^0$, respectively. In component form, with respect to a orthonormal Cartesian base where axis 1 is longitudinal and axis 2 is transverse and directed to the top surface, these are

$$\boldsymbol{n}^0 = \left(-\sin\theta_1, \cos\theta_1\right) \quad \text{and} \quad \boldsymbol{m}^0 = \left(\cos\theta_1, \sin\theta_1\right). \tag{2.1}$$

In each phase, $\boldsymbol{E}$ and $\boldsymbol{D}$ designate electric and electric displacement fields, respectively, whereas the total stress is denoted by $\boldsymbol{S}$. With the assumption of the absence of both volume charges and body forces, the governing equations are

$$\mathrm{div}\boldsymbol{S} = \boldsymbol{0}, \quad \mathrm{div}\boldsymbol{D} = 0, \quad \mathrm{curl}\boldsymbol{E} = \boldsymbol{0}, \tag{2.2}$$

where the last equation implies that $\boldsymbol{E}$ can be derived from the electrostatic potential $\phi(\boldsymbol{x})$ such that $\boldsymbol{E} = -\mathrm{grad}\,\phi(\boldsymbol{x})$. The electric quantities follow the relationship of an ideal dielectric, $\boldsymbol{D} = \varepsilon\boldsymbol{E}$, where ε is the permittivity of the material that is independent of strain. Continuity across the interfaces between '*a*' and '*b*' can be enforced by imposing the following jump conditions

$$\boldsymbol{n}^0 \cdot [\![\boldsymbol{D}]\!] = 0, \quad \boldsymbol{n}^0 \times [\![\boldsymbol{E}]\!] = \boldsymbol{0}, \quad [\![\boldsymbol{S}]\!]\boldsymbol{n}^0 = \boldsymbol{0}, \; \boldsymbol{m}^0 \cdot ([\![\boldsymbol{e}]\!]\boldsymbol{m}^0) = 0; \tag{2.3}$$

in $(2.3)_4$, $\boldsymbol{e}$ denotes the strain tensor. The brackets $[\![\cdot]\!]$ indicate the jump across the interfaces and are defined as $[\![f]\!] = f^a - f^b$.

Under the assumption of a homogeneous response in each phase, we can define the macroscopic average quantities in the whole composite as a sum of the weighed quantities in each phase. We thus define the average quantities as

$$\boldsymbol{E}^{\mathrm{av}} = c^a\boldsymbol{E}^a + c^b\boldsymbol{E}^b, \quad \boldsymbol{S}^{\mathrm{av}} = c^a\boldsymbol{S}^a + c^b\boldsymbol{S}^b, \quad \boldsymbol{e}^{\mathrm{av}} = c^a\boldsymbol{e}^a + c^b\boldsymbol{e}^b. \tag{2.4}$$

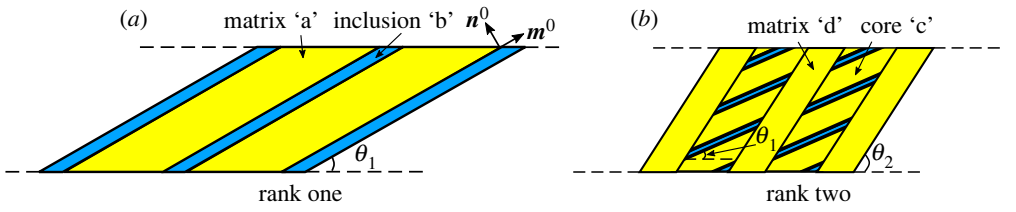

Figure 1. Sketch of a rank-one (*a*) and a rank-two (*b*) laminated dielectric elastomer composite.

We can express the jump condition $(2.3)_2$ in an alternate form, i.e.

$$\boldsymbol{E}^a - \boldsymbol{E}^b = \beta \boldsymbol{n}^0, \tag{2.5}$$

where β is a real parameter. We can thus obtain expressions to relate the singular phases to the average quantity using equation $(2.4)_1$, namely

$$\boldsymbol{E}^a = \boldsymbol{E}^{\mathrm{av}} + c^b \beta \boldsymbol{n}^0 \quad \text{and} \quad \boldsymbol{E}^b = \boldsymbol{E}^{\mathrm{av}} - c^a \beta \boldsymbol{n}^0. \tag{2.6}$$

An analogous procedure is followed for the mechanical problem giving us the expressions

$$\left.\begin{aligned} \boldsymbol{e}^a &= \boldsymbol{e}^{\mathrm{av}} - \omega_1 c^b (\boldsymbol{m}^0 \otimes \boldsymbol{n}^0 + \boldsymbol{n}^0 \otimes \boldsymbol{m}^0) - \omega_2 c^b \boldsymbol{n}^0 \otimes \boldsymbol{n}^0 \\ \text{and} \qquad \boldsymbol{e}^b &= \boldsymbol{e}^{\mathrm{av}} + \omega_1 c^a (\boldsymbol{m}^0 \otimes \boldsymbol{n}^0 + \boldsymbol{n}^0 \otimes \boldsymbol{m}^0) + \omega_2 c^a \boldsymbol{n}^0 \otimes \boldsymbol{n}^0, \end{aligned}\right\} \tag{2.7}$$

where ω_1 and ω_2 are unknown real parameters.

The constitutive equations should describe a linear electro-elastic isotropic material. To this end, we refer to the analysis by McMeeking & Landis [25] by assuming the following relationships in terms of total stress in each phase

$$\left.\begin{aligned} S^a_{ij} &= 2G^a e^a_{ij} + \left(B^a - \frac{2G^a}{3}\right) e^a_{kk}\delta_{ij} + \varepsilon^a E^a_i E^a_j - \frac{\varepsilon^a}{2} E^a_k E^a_k \delta_{ij} \\ \text{and} \qquad S^b_{ij} &= 2G^b e^b_{ij} + \left(B^b - \frac{2G^b}{3}\right) e^b_{kk}\delta_{ij} + \varepsilon^b E^b_i E^b_j - \frac{\varepsilon^b}{2} E^b_k E^b_k \delta_{ij}, \end{aligned}\right\} \tag{2.8}$$

where G and B are the shear and bulk moduli of the relevant material, respectively, and δ_{ij} represents the Kronecker delta. Note that the r.h.s. of the above expressions can be split into the elastic (first two terms) and electrostatic (last two terms) stresses that are independent of each other.

We consider composite elastomer membranes which experience electric actuation across their thickness (i.e. $E^{\mathrm{av}}_1 = 0$) that are subjected to two types of mechanical boundary conditions. The first one is called 'aligned loading', in which the macroscopic shear strain is imposed to vanish as well as the normal components of the total stress, namely

$$e^{\mathrm{av}}_{12} = 0, \quad S^{\mathrm{av}}_{11} = S^{\mathrm{av}}_{22} = 0. \tag{2.9}$$

In the second condition, the external boundary of the membrane is traction-free, then

$$\boldsymbol{S}^{\mathrm{av}} = \boldsymbol{0}, \tag{2.10}$$

is imposed throughout the device.

For all problems addressed, the solution is obtained in closed-form with the help of the software Mathematica (Wolfram Research, Inc.). For rank-two laminates, the method to achieve the final condition to be solved is detailed in the Appendix. We conclude by recalling that the microscopic electric fields $\boldsymbol{E}^a$ and $\boldsymbol{E}^b$ can be easily obtained, once the problem is solved, through equations $(2.4)_1$ and (2.6). A similar explicit calculation is performed in [20].

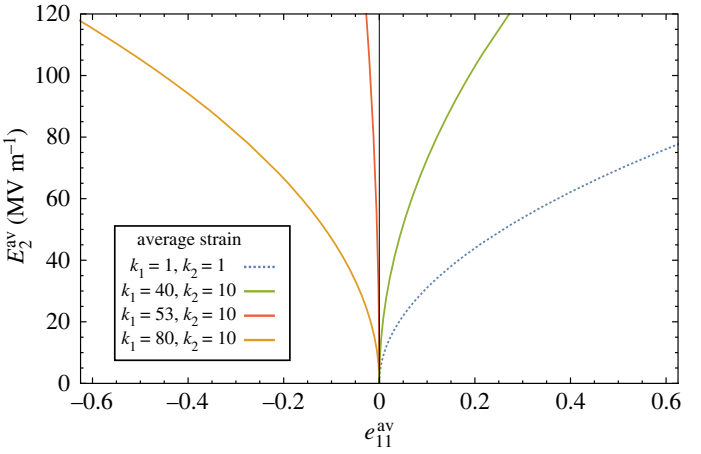

Figure 2. Rank-one actuation under 'aligned loading'. Actuation response for $k_2 = 10$, $c^a = 0.8$, $\theta_1 = 30^\circ$ at varying k_1; the homogeneous response (i.e. $k_1 = k_2 = 1$) is plotted with a dashed line. The curves on the right-hand part ($e_{11}^{av} > 0$) denote elongation, those on the left-hand part ($e_{11}^{av} < 0$) contraction.

3. Rank-one laminated composite

(a) Actuation under 'aligned loading' boundary conditions

We first undertake the investigation of the occurrence of the new modes for a rank-one laminate starting from the more restrictive 'aligned loading' boundary conditions, equations (2.9).

By assuming an ideal dielectric, we obtain the parameter β using both jump condition in $\boldsymbol{D}$ (equation $(2.3)_1$) and equation (2.5). Similarly, ω_1 and ω_2 are calculated from the jump in $\boldsymbol{S}$ (equation $(2.3)_3$), with the stress in each phase given by equations (2.8). Once the parameters are calculated, the average strain $\boldsymbol{e}^{av}$ is achieved through boundary conditions where $\boldsymbol{S}^{av}$ is provided by equations $(2.4)_2$ and (2.8).

To define the actuation response, we need to set material parameters for the two phases. To this end, we first replace the bulk modulus with Poisson's ratio ν with the well-known relationship

$$B = \frac{2G(1+\nu)}{3(1-2\nu)}.$$

As elastomers are typically close to being incompressible, a high Poisson's ratio is chosen for both phases, i.e. $\nu^a = \nu^b = 0.495$. To analyse the response to actuation we then fix the material parameters for the soft matrix to typical values of $G^a = 100$ kPa and $\varepsilon^a = 4.68\,\varepsilon_0$, where $\varepsilon_0 = 8.85 \times 10^{-12}$ Fm^{-1}. The stiffer material will then have its parameters defined by $\varepsilon^b = k_1\varepsilon^a$ and $G^b = k_2 G^a$, where k_1 and k_2 are dimensionless constants.

Figure 2 illustrates the response of a rank-one laminate ($k_2 = 10$, $c^a = 0.8$, $\theta_1 = 30^\circ$) for different contrast k_1. At an increase of the latter parameter, the response modifies and from longitudinal *elongation* it transitions to the unconventional one, i.e. longitudinal *contraction*. For comparison, the response of a homogeneous material (i.e. $k_1 = k_2 = 1$) is also sketched with a dashed line.

Figure 3 shows the domains where the two actuation modes occur in a plot where k_1 varies with the lamination angle θ_1. The drawn curves set the absence of longitudinal strain, $e_{11}^{av} = 0$ (i.e. *no longitudinal actuation at all*), for two different shear moduli ratios, $k_2 = 10$ and 100. In both cases, the volume fraction of the composite is set to $c^a = 0.8$. The optimum value of the lamination angle which enhances the unconventional behaviour is approximately 30° for both values of k_2. The two curved lines share an asymptote at $\theta_1 \approx 45^\circ$ (above this angle the actuation can be only the conventional one) and are very close to each other. The latter circumstance means that the leading

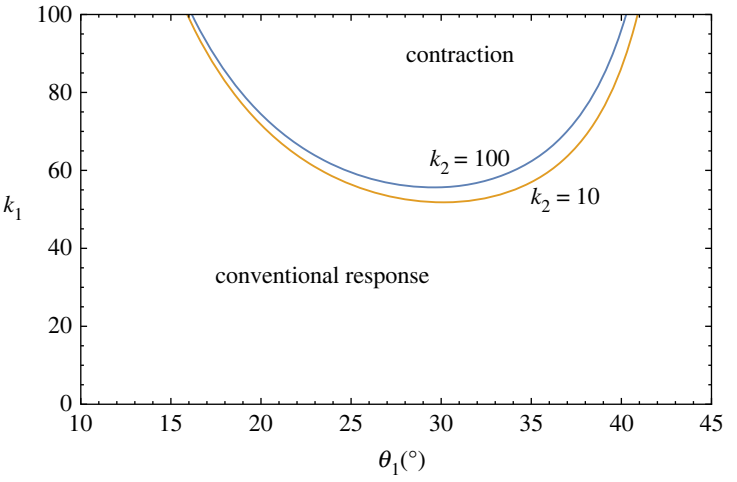

Figure 3. Rank-one actuation under 'aligned loading'. Domains showing the actuation behaviour as k_1 and θ_1 are varied. Orange and blue curves indicate inversion of the responses for $k_2 = 10$ and $k_2 = 100$, respectively. Both composites have a volume fraction of $c^a = 0.8$.

material parameter that set the behaviour of the laminate is the ratio of permittivities k_1, with k_1 being approximately 50–60 when the lamination angle is close to optimum.

To better comprehend how the switch between elongation and contraction occurs, we analyse local rotation and stretching of each phase. For our examination we select the geometric and material parameters of $\theta_1 = 30^\circ$, $k_2 = 10$ and $c^a = 0.8$, and try to represent how the two materials deform as we increase the permittivity ratio k_1. Strains are computed through equation (2.7); we then calculate the vector of principal strains $\hat{e}$ and the angle α, taken w.r.t. the longitudinal direction (i.e. axis 1), which singles out the principal directions of strain. In particular, the latter is given by

$$\tan(2\alpha) = \frac{2e_{12}}{e_{11} - e_{22}}. \tag{3.1}$$

As a way to select the value of the electric fields, the elastomer is subjected to the external macroscopic field $E_2^{\mathrm{av}} = 100\,\mathrm{MV\,m^{-1}}$. Figure 4 shows how angle α varies with k_1 in each phase and, similarly, figure 5 reports the principal strains. It is to note that for the chosen parameters the transition between responses occurs at a value of $k_1 \approx 51.812$. The figures show that the principal directions rotate dramatically about this value, coupled with the principal strains reaching their minima in absolute value. As we move away from the transition value, each material in the composite tends to stabilize in its response, showing linear behaviour of the strains and constant angle α. To better illustrate the underlying mechanisms, figure 6 displays how a unit cell deforms as k_1 increases. The deformed unit cell is sketched with the axes aligned with the principal directions of strain; therefore, the angle of inclination corresponds to α, whereas the lengths of the sides are proportional to the principal strains $\hat{e}_{11}$ and $\hat{e}_{22}$.

The first set of cases concerns $\theta_1 = 30^\circ$. At low values of k_1 the conventional response appears clearly, with both materials elongating longitudinally. The matrix experiences almost no rotation whereas the direction of the highest principal strain of the stiff inclusion is inclined of about 24°. At an increase of the permittivity ratio, the principal directions of the inclusion start to rotate clockwise until they stabilize at an angle of about -65°, with those of the matrix material rotating counter-clockwise up to an angle of approximately 87°. During this rotation the strains are relatively small and the leading cause of the transition to the non-conventional response is rotation of the principal directions of strain. When looking at a high value of k_1, e.g. $k_1 = 70$, both phases are clearly rotated in such a way that the macroscopic elongation occurs transversally. In

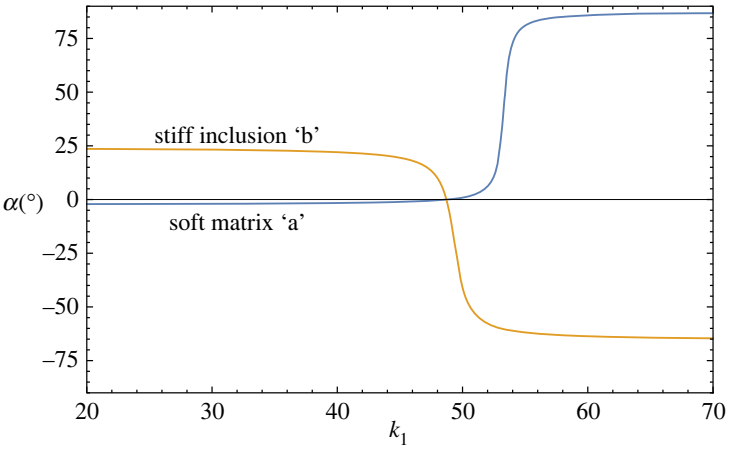

Figure 4. Rank-one actuation under 'aligned loading'. Principal strain orientation angles of the two phases as k_1 is varied. Blue and orange curves represent the soft and the stiff phase, respectively. Parameters of $\theta_1 = 30^\circ$, $k_2 = 10$ and $c^d = 0.8$ are adopted; the elastomer is actuated with $E_2^{\text{av}} = 100$ MV m^{-1}.

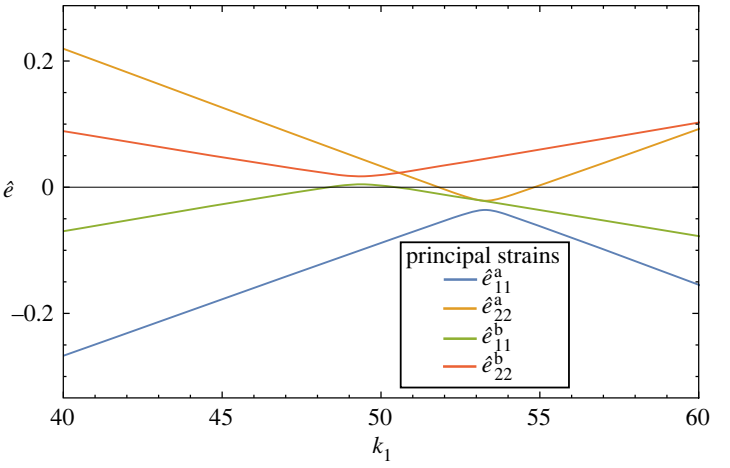

Figure 5. Rank-one actuation under 'aligned loading'. Principal strains of the two phases as k_1 is varied. Parameters of $\theta_1 = 30^\circ$, $k_2 = 10$ and $c^d = 0.8$ are adopted; the elastomer is actuated with $E_2^{\text{av}} = 100$ MV m^{-1}.

the neighbourhood of the transition value of $k_1 \approx 51.812$ large changes in rotation occur at very small changes of k_1 in both constituents, with the stiff inclusion leading the matrix. Moreover, we note that at $k_1 \approx 48.711$, because of the 'aligned' boundary conditions, there is a point in which both angles α vanish and, as a consequence, so are shear strains in each phase.

Lamination angles $\theta_1 = 10^\circ$ and $\theta_1 = 50^\circ$ are also investigated in figure 6 to represent configurations for which the change in longitudinal actuation does not occur. For both, the response of the two selected composites (i.e. $k_1 = 20,\ 70$) is elongation and is almost independent of the contrast k_1.

(b) Actuation under traction-free boundary conditions

We next examine boundary conditions where shear strains are not limited. The analysis follows the previous one with the difference being that no constraint are specified on the average strain and equation (2.10) are used. The same material and geometrical parameters adopted in the previous section are selected and similar figures plotted.

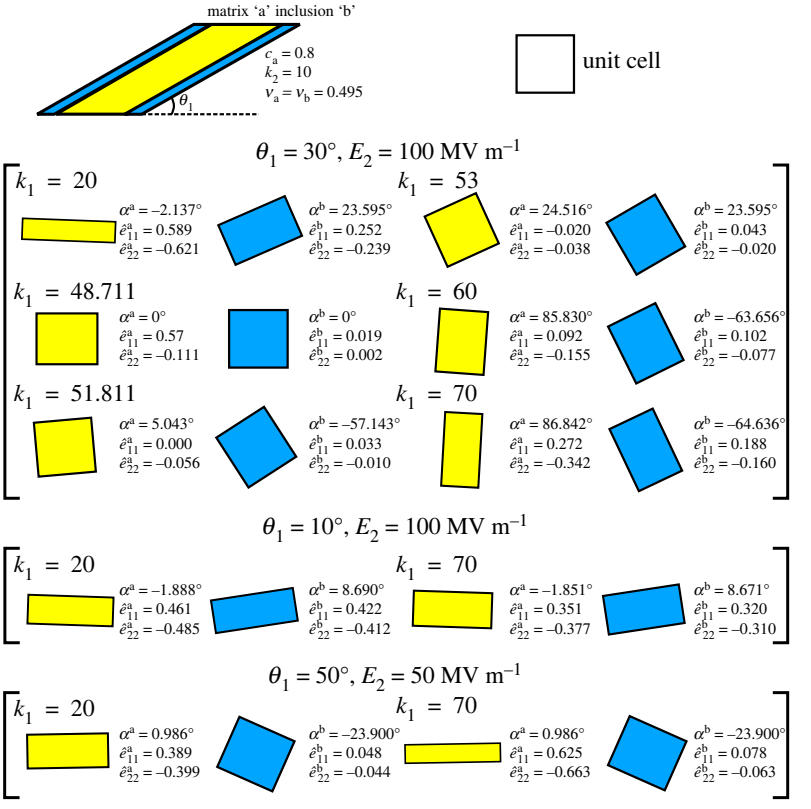

Figure 6. Rank-one actuation under 'aligned loading'. Diagram showing how a unit cell of each material phase is deformed and rotated for increasing values of k_1. Parameters of $k_2 = 10$ and $c^a = 0.8$ are adopted for all cases; from top to bottom: $\theta_1 = 30°$, $E_2^{av} = 100$ MV m^{-1}, $\theta_1 = 10°$, $E_2^{av} = 100$ MV m^{-1} and $\theta_1 = 50°$, $E_2^{av} = 50$ MV m^{-1} are displayed.

Figure 7 summarizes the findings for this relevant case. We note first that, differently from before, the minimum value of k_1 at which contraction occurs is strongly dependent on the contrast in shear moduli. In comparison with the 'aligned loading' case, for $k_2 = 10$ and $\theta_1 = 30°$ the value of k_1 to expect contraction is almost doubled, $k_1 = 99.62$, whereas for $k_2 = 100$ it is larger than 500. A second outcome is that the minimum of the curves displayed in the figure (i.e. optimum angle of the laminate) also depends on the contrast in shear moduli: it ranges from approximately 30° for $k_2 = 1$ to 18° for $k_2 = 100$. However, as before, there is an asymptotic behaviour for all curves at $\theta_1 \approx 45°$.

Figures 8 and 9 deal with orientation of principal direction of strains and principal strains as a function of k_1. With fewer restraints imposed by the current boundary conditions, about the transition value of $k_1 = 99.62$ there is no drastic change in orientation of principal directions. Unlike before, both material phases rotate clockwise, with the stiff inclusion rotating remarkably right from the start and the soft material phase undergoing a much longer drawn out rotation as k_1 increases. The functions of the two angles intersect at a value of $k_1 = 14.155$; however, this happens at an angle of $-14.64°$ unlike previously, where they both aligned at 0°. Looking at the principal strains does not provide much insight to the occurrence of the response transition. The strains in the stiff inclusion seem to have a minimum of their principal value at $k_1 = 14.214$, about the value where the orientation angles intercept. However, this is far from the transition value, where the curves of principle strains show a linear trend. Looking at both graphs we can understand that the transition occurs because of an interplay between the slowly rotating soft bulk material coupled with the material experiencing higher strains.

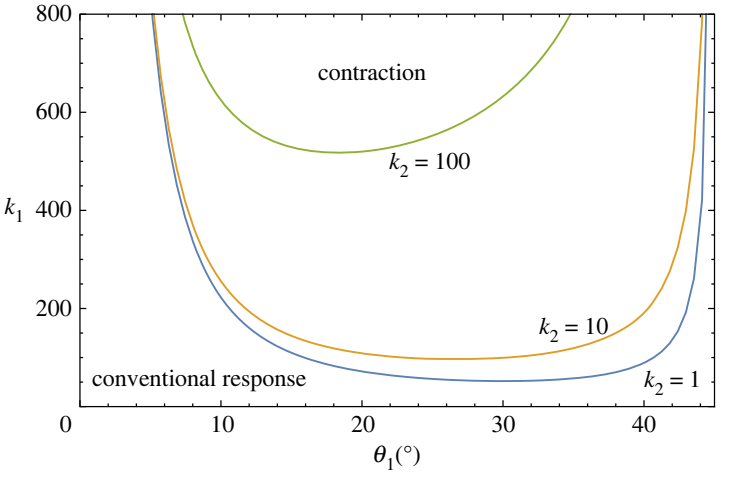

Figure 7. Rank-one actuation under traction-free conditions. Domains showing inversion of actuation behaviour as k_1 and θ_1 are varied. The three curves show responses for $k_2 = 1$, 10 and 100. The three composites have a volume fraction of $c^a = 0.8$.

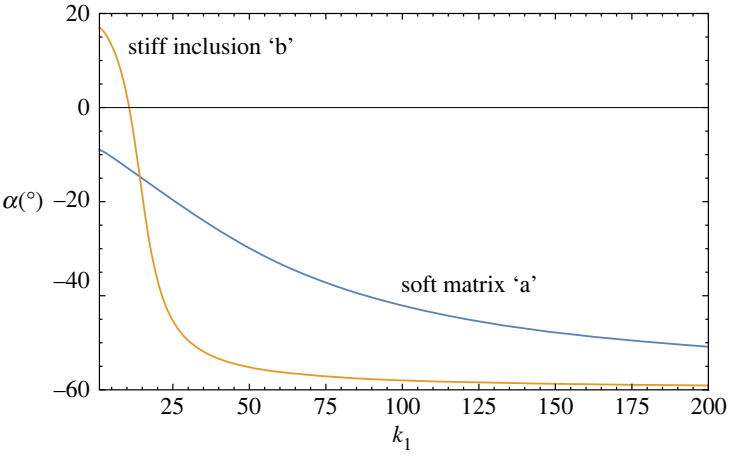

Figure 8. Rank-one actuation under traction-free conditions. Angles defining the principal directions of strain of the two phases as k_1 is varied. Blue and orange curves represent the soft and stiff phase, respectively. Parameters of $\theta_1 = 30^\circ$, $k_2 = 10$ and $c^a = 0.8$ are adopted; the elastomer is actuated with $E_2^{av} = 100$ MV m^{-1}.

There are also some additional behaviours to note that are not highlighted in the figures. When the shear strains are not limited, the composite experiences high values of shear strain, which makes it the dominant deformation.

4. Rank-two laminated composites

(a) Homogenization of rank-two laminates

The goal of this section is to assess if a rank-two laminate can (i) confirm and—possibly—(ii) enhance the behaviour of the previously discussed rank-one composite. Because of the electro-elastic small-strain setting, we follow the work done by Tian [26] and Tevet-Deree [27] that introduced an iterative procedure to compute the effective response of a laminate with a generic rank.

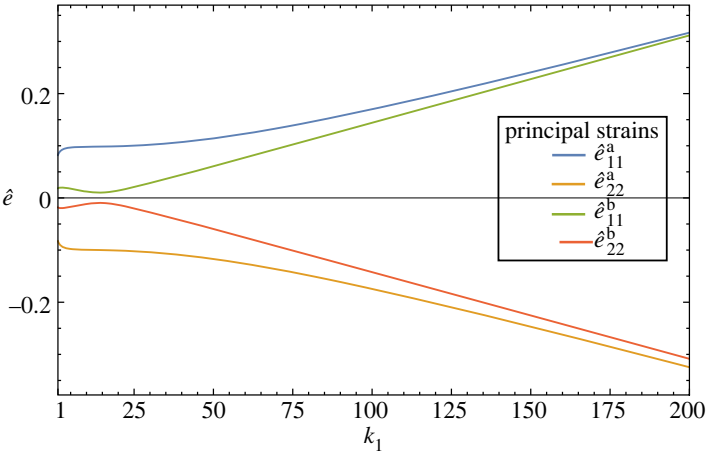

Figure 9. Rank-one actuation under traction-free conditions. Principal strains of the two phases as k_1 is varied. Parameters of $\theta_1 = 30^\circ$, $k_2 = 10$ and $c^a = 0.8$ are adopted; the elastomer is actuated with $E_2^{\text{av}} = 100$ MV m^{-1}.

Figure 1*b* shows a sketch of the composite under investigation that is made up of a core phase, which is a rank-one material with soft and stiff materials, and an—outer—matrix phase which consists of the same soft material. The core has a lamination angle of θ_1, that is independent of θ_2, which in turn describes the grade of the matrix. The field equations to be satisfied in each phase are still $(2.2)_{1,2}$; however, now it is convenient to write the constitutive equations as

$$\boldsymbol{D} = \boldsymbol{M}\boldsymbol{E}, \quad \boldsymbol{S} = \mathbb{C}\boldsymbol{e} + \mathbb{A}\boldsymbol{E} \otimes \boldsymbol{E}, \tag{4.1}$$

where $\boldsymbol{M}$ is the second-order tensor of dielectric moduli, while $\mathbb{C}$ and $\mathbb{A}$ are the fourth-order tensors of elastic moduli and electromechanical coupling, respectively. For a homogeneous phase, their non-zero components are

$$\begin{aligned}
&C_{1111} = C_{2222} = B + \frac{4G}{3}, \quad C_{1122} = C_{2211} = B - \frac{4G}{3},\\
&C_{1212} = C_{1221} = C_{2112} = C_{2121} = G,\\
&A_{1111} = A_{2222} = \frac{\varepsilon}{2}, \quad A_{1122} = A_{2211} = -\frac{\varepsilon}{2}, \quad A_{1212} = A_{1221} = A_{2112} = A_{2121} = \frac{\varepsilon}{2},\\
&M_{11} = M_{22} = \varepsilon.
\end{aligned} \tag{4.2}$$

To deal with homogenization of sub-rank laminates, we also introduce the electrostatic and elastic concentration tensors $\boldsymbol{g}$ and $\mathbb{G}$, respectively, relating the fields in each phase to the average ones in the composite, componentwise

$$E_i = g_{ij}E_j^{\text{av}}, \quad e_{ij} = G_{ijkl}e_{kl}^{\text{av}}. \tag{4.3}$$

It has been shown in [16] that the effective coupling and elastic moduli tensors for a rank—N material can be obtained using the expressions

$$A_{ijkl}^{\text{av}} = \sum_{r=1}^{N} c^{(r)} A_{mnpq}^{(r)} G_{mnij}^{(r)} g_{pk}^{(r)} g_{ql}^{(r)} \quad \text{and} \quad C_{ijkl}^{\text{av}} = \sum_{r=1}^{N} c^{(r)} C_{ijpq}^{(r)} G_{pqkl}^{(r)}. \tag{4.4}$$

These effective coupling tensors allow us to calculate the effective macroscopic strain tensor. By using equation $(4.1)_2$, we obtain the relationship

$$e_{ij}^{\text{av}} = C_{abij}^{\text{av}^{-1}} (A_{abkl}^{\text{av}} E_k^{\text{av}} E_l^{\text{av}}), \tag{4.5}$$

which lets us compute the strain knowing just elastic moduli and coupling tensors. As $\mathbb{C}^{\mathrm{av}^{-1}}$ may be hard to calculate, in the Appendix we provide a method to solve this equation. It may also be useful to have at hand the effective dielectric moduli, given by

$$\boldsymbol{M}^{\mathrm{av}} = \sum_{r=1}^{N} c^{(r)} \boldsymbol{M}^{(r)} \boldsymbol{g}^{(r)}. \tag{4.6}$$

(b) Transition to contraction actuation mode in rank-two laminates

We analyse a rank-two laminate where the matrix is the same as the soft material in the core. The equivalent properties of the core will be indicated by subscript c whereas those of the matrix by subscript d, so that the relevant volume fractions satisfy the expression $c_c + c_d = 1$. To compare the performance of a rank-two composite to that of a simple laminate, we define an equivalent volume fraction c_{eq}, which would be the rank-one volume fraction c_a to achieve the same overall percentage of soft to stiff material in the two composites. The volume fractions of the current composite relate to the rank-one equivalent by

$$(1 - c_a)c_c = 1 - c_{\mathrm{eq}}. \tag{4.7}$$

By fixing c_{eq} one can obtain c_a and vice-versa. To obtain a solution in terms of strain for the rank-two composite, we first follow the procedure set for the simple laminate, explained in §3a, to achieve parameters β, ω_1 and ω_2.

The boundary conditions adopted are traction-free, therefore, comparison of performance is carried out with results from §3b for the simple laminate. The various tensors $\boldsymbol{g}$, $\mathbb{C}$, $\mathbb{G}$ and $\mathbb{A}$ are determined from equations (2.6) and (2.8) for each phase of the core. These are then inserted in equations (4.4) and (4.6) to obtain the effective coupling and moduli tensors for the core material. As a rank-one layout is recovered if the core is all filled with the stiff material, we have checked that equation (4.5) provides identical strains to those determined previously for a simple laminate. For all the analyses, we confirm the material parameters already adopted, namely $G^a = G^d = 100$ kPa and $\varepsilon^a = \varepsilon^d = 4.68\,\varepsilon_0$. The stiff material is again defined by variables k_1 and k_2.

When comparing actuation strains for the two types of composites, by adopting for example values either $k_1 = k_2 = 10$ or $k_1 = k_2 = 100$, data in full agreement with that calculated in [16,19,20,28] have been attained.

For our goal of enhancing the transition between longitudinal elongation and contraction, we note that for the rank-two composite we can take advantage of the fact that multiple parameters that can be varied independently come into play. In this section, we define an 'optimum' rank-two laminate having the various parameters combined to minimize k_1 at the transition between conventional and unconventional responses. The lamination angles greatly affect this minimization, other parameters being equal, as shown in figures 10 and 11. Both of these figures are for a rank-two composite with $c_{\mathrm{eq}} = 0.5$ and $c_d = 0.1$ which is compared to the simple laminate with $c_a = 0.5$ and optimum angle $\theta_1 = 30^\circ$.

In the former figure, the grades of the two laminates are set by angles $\theta_1 = 30^\circ$ and $\theta_2 = 25^\circ$, a choice that is not related to any optimization. Here, the simple laminate exhibits the inversion at lower values of variable k_1 over the whole domain. It is also evident in the figure that the domain of inversion of actuation for the rank-two composite is a region located on the left-hand side of the diagram for which there is no change in actuation for relatively large values of k_2 ($k_2 > 28$). This occurs for $\theta_1 > \theta_2$, whereas an enhanced performance is found for the opposite case, namely $\theta_2 > \theta_1$. When the two angles coincide, matrix and core align with each other and the rank-one response is captured.

Figure 11 shows a response for a rank-two composite in which the angles are optimized. For this type of configuration, the curve of inversion is almost flat and has a horizontal asymptote as k_2 increases. The parameters are selected ($\theta_1 = 48^\circ$ and $\theta_2 = 93^\circ$) to lower this asymptote such that the transition between elongation and contraction appears with as low a k_1 as possible.

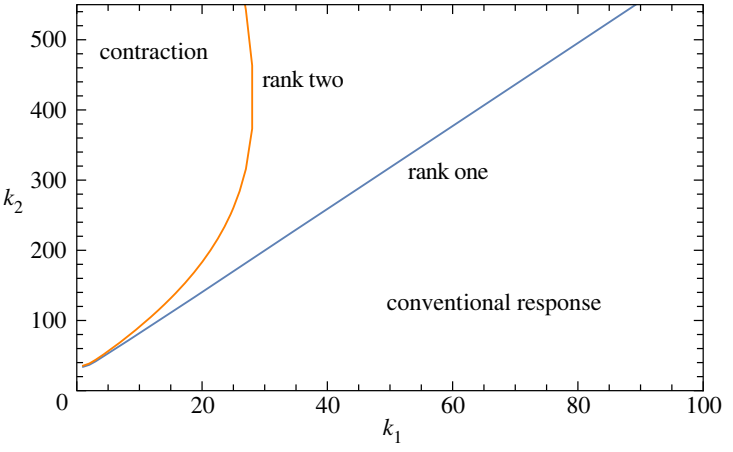

Figure 10. Domains showing the actuation behaviour and lines of inversion for rank-one and rank-two composites. Volume fractions are $c_a = 0.5$ for the former and $c_{eq} = 0.5$, $c_d = 0.1$ for the latter. The adopted lamination angles are $\theta_1 = 30^\circ$ for the simple laminate (the optimal value) and $\theta_1 = 30^\circ$, $\theta_2 = 25^\circ$ for the rank-two one.

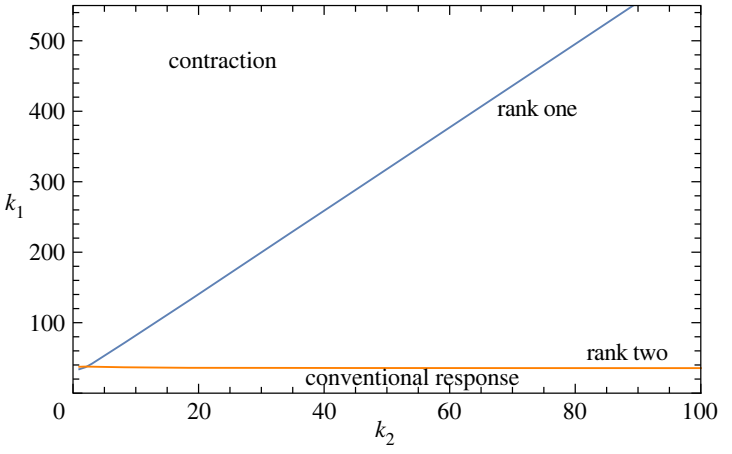

Figure 11. Domains showing inversion of actuation for rank-one and rank-two composites with optimum parameters for both. Volume fractions are $c_a = 0.5$ for the former and $c_{eq} = 0.5$, $c_d = 0.1$ for the latter. The adopted lamination angles are $\theta_1 = 30^\circ$ for the simple laminate and $\theta_1 = 48^\circ$, $\theta_2 = 93^\circ$ for the rank-two one.

Figure 12 displays a similar picture with optimum parameters chosen for $c_{eq} = 0.84$ and $c_d = 0.17$. For the rank two they are $\theta_1 = 50^\circ$ and $\theta_2 = 95^\circ$, whereas the usual $\theta_1 = 30^\circ$ is adopted for the simple laminate. The enhanced response is very similar to that determined for the previous configuration with a higher percentage of stiff material, as the graph is only shifted upwards.

Figure 13 shows how the volume fraction of the rank-two laminate, with a given equivalent fraction, relates to the value of k_1 needed for the inversion of actuation. In this analysis the contrast in shear moduli, k_2, is set to 100 as this is representative of the horizontal asymptote displayed in previous figures for 'optimum' laminates. For each value of c_d, the lamination angles needed to be duly computed to give the lowest possible value k_1. When $c_d \to 0$ and $c_d = c_{eq}$ the composite exhibits the response of the simple laminate. This is expected as either the matrix vanishes or the core has to be made up of only the stiff material. The figure shows that for all the volume fractions in between these two limits the optimized rank-two laminate exhibits the inversion of actuation

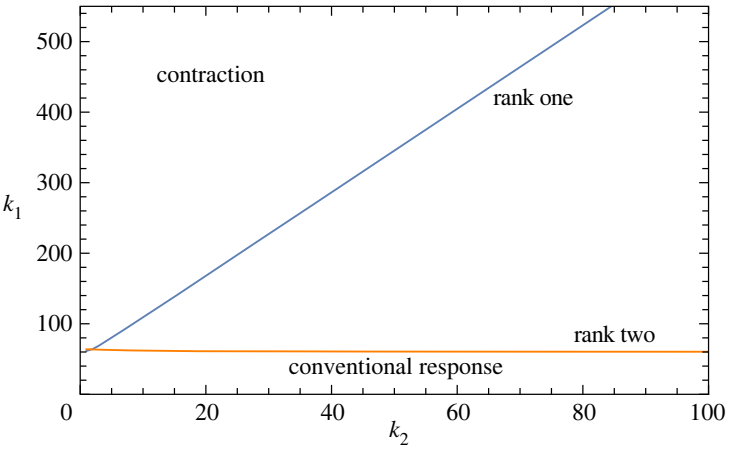

Figure 12. Domains showing inversion of actuation for rank-one and rank-two composites with optimum parameters for both. Volume fractions are $c_a = 0.84$ for the former and $c_{eq} = 0.84$, $c_d = 0.17$ for the latter. The adopted lamination angles are $\theta_1 = 30^\circ$ for the simple laminate and $\theta_1 = 50^\circ$, $\theta_2 = 95^\circ$ for the rank-two one.

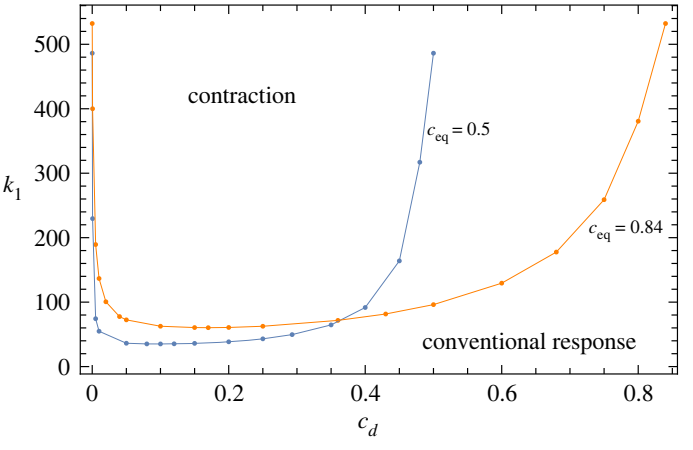

Figure 13. Domains showing the actuation behaviour and lines of inversion for optimum rank-one and rank-two composites for cases $c_{eq} = 0.5$ and 0.84 as c_d is varied against k_1. A value of $k_2 = 100$ is adopted. Lamination angles are optimized for each computed case.

for lower values of k_1 as compared to the best rank-one composite. The optimum matrix volume fraction c_d is shown to be 0.1 and 0.17 for an equivalent fraction c_{eq} of 0.5 and 0.84, respectively. Overall, this analysis shows that to create a rank-two composite capable of enhancing contraction, parameters to start the iterative optimization procedure are a volume fraction for the matrix of about 0.1–0.2 and lamination angles of $\theta_1 \approx 50^\circ$ and $\theta_2 \approx 95^\circ$.

We next analyse longitudinal and shear strains in both layouts to better understand their actuation performance. We define the effective strain tensors as $\boldsymbol{e}^1$ and $\boldsymbol{e}^2$ for rank-one or rank-two composites, respectively. To analyse the strains we use the parameters of the composite adopted in figure 12 ($\theta_1 = 50^\circ$, $\theta_2 = 95^\circ$) with $c_{eq} = 0.84$; we fix a value of k_2 and range k_1, actuating both composites with a macroscopic electric field of $E_2^{av} = 100\,\mathrm{MV\,m^{-1}}$. Figure 14 displays the outcome with parts (*a*) and (*b*) corresponding to $k_2 = 5$ and $k_2 = 20$, respectively. The main difference between the rank-one and rank-two composites is that for both shear and longitudinal strains

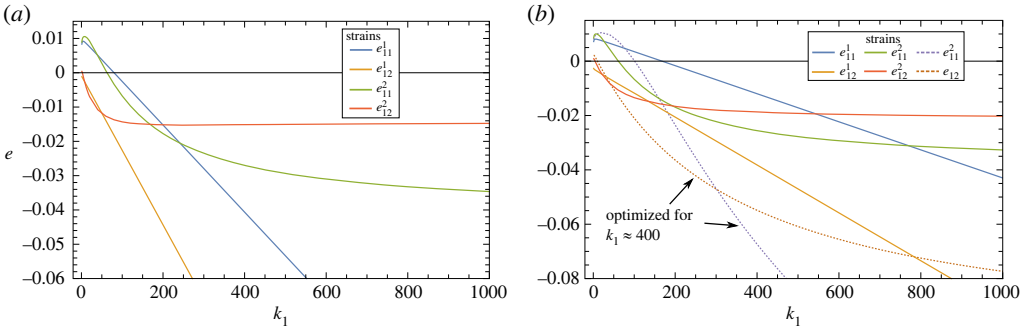

Figure 14. Strain components sketched against k_1 of rank-one and rank-two laminates actuated with $E_2^{\text{av}} = 100\,\text{MV m}^{-1}$. Optimum parameters are adopted with $c_{\text{eq}} = 0.84$. (*a*) $k_2 = 5$, (*b*) $k_2 = 20$.

the latter exhibits horizontal asymptotes at large k_1 whereas for the former they increase almost linearly. We will focus in our ensuing comments on permittivity ratios k_1 up to ≈ 500.

In part (*a*), with the contrast in shear moduli being relatively low, up to the point at which the responses of the two composites diverge, their strains are quite similar, as similar are the values of k_1 of the transition between elongation and contraction. This is no longer verified for longitudinal strains in part (*b*), that is for a higher stiffness contrast. In this diagram, the rank-two outperforms the simple laminate both in elongation and contraction strains. Under the conventional, elongation regime this is expected as this is the actuation type where hierarchical laminates have been thoroughly investigated in previous studies [16,18,20,29]. Our work confirms that this is also the case when the composite displays the contraction actuation mode. We also note that shear strains are, in magnitude, of the same order of the longitudinal ones.

In both plots of figure 14, the computed strains are for *layouts computed to minimize the value of* k_1 *at the transition* as determined, e.g. in figure 12. However, a relevant problem is the following: how to reach the maximum contraction given the type of constituents? As an example, in figure 12*b* we select $k_1 = 400$ and compute the configuration to achieve the lowest possible longitudinal strain. The parameters are: $c_{\text{eq}} = 0.84$, $c_d = 0.05$, $\theta_1 = 56^\circ.10$, $\theta_2 = 95^\circ.35$, and the strain at $E_2^{\text{av}} = 100\,\text{MV m}^{-1}$ amounts approximately to -0.065. This example demonstrates that once we know that longitudinal contraction is possible with the phases at hand, the optimum configuration should be carefully determined according to the design requirements of the device.

Figure 15 reports two diagrams where the longitudinal strain is sketched against the two lamination angles for a rank-two composite (volume fractions are $c_d = 0.17$ and $c_{\text{eq}} = 0.84$). It is notable that when $\theta_1 = \theta_2$ the behaviour of the simple laminate is recovered, highlighted in both plots with a blue line. The minima of the surfaces are marked with green and blue dots, for the rank-two and rank-one layouts, respectively. The two figures have different material ratios: $k_1 = 300$ and $k_2 = 20$ for part (*a*) and $k_1 = 300$ and $k_2 = 300$ for part (*b*). The composite is actuated with a field $E_2^{\text{av}} = 10\,\text{MV m}^{-1}$.

Figure 15*a* highlights that when $k_2 < k_1$, a simple laminate always performs better in elongation than the rank-two configuration, irrespectively of the grade of phases of the latter. However, the maximum strain in contraction for optimized configurations of the rank-two layout (i.e. the minima of the surface that have a negative value) are always larger than those associated with the simple laminate. In figure 15*b*, the same material ratios are selected, $k_1 = k_2 = 300$. Here, optimized rank-two configurations perform better for both elongation and contraction. The simple laminate deforms always with positive longitudinal strain. Overall, the rank-two composite can outperform the simple laminate, but a careful study of geometry and material parameters needs to be undertaken as the results may vary greatly, being very sensible to small changes of the quantities involved. To complete the analysis, we report that the coordinates of minima for the rank-two in (a) are $\theta_1 = 57^\circ.98$, $\theta_2 = 85^\circ.08$ (the minimum is -0.0364) whereas in

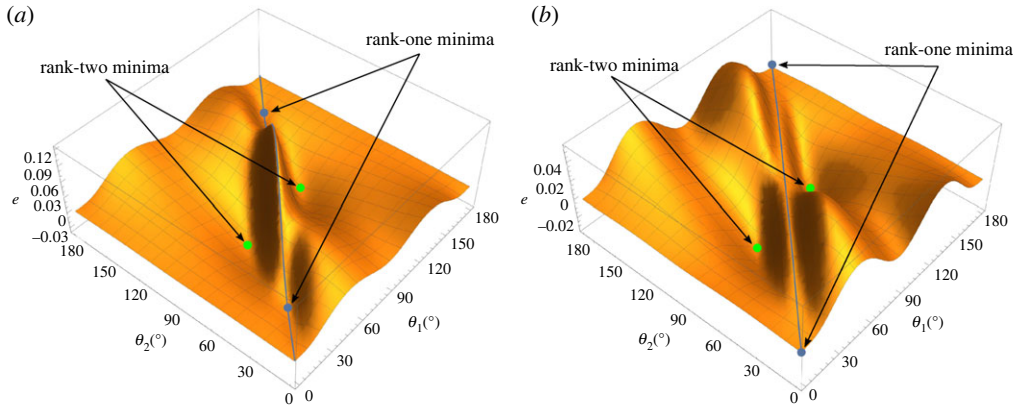

Figure 15. Plot of the longitudinal strain for rank-two laminates as θ_1 and θ_2 are varied for $c_d = 0.17$, $c_{eq} = 0.84$. The blue line shows the loading path for a simple laminate with the dots marking the minimum strains. The material is actuated with $E_2^{av} = 10$ MV m^{-1}. (*a*) $k_1 = 300$, $k_2 = 20$, (*b*) $k_1 = k_2 = 300$.

(b) they are $\theta_1 = 59^\circ.13$, $\theta_2 = 86^\circ.63$ (value of the minimum: -0.0344) (in both diagrams points are doubled as there is a symmetry with respect to the right angle).

5. Viability given currently available materials

The investigation carried out so far was undertaken by changing the material parameters k_1 and k_2 to show the whole range of responses for both rank-one and rank-two laminates. However, a non-secondary aspect to be considered is to know the current availability of materials to be in principle employed to assess the viability of such composite devices able to display a 'non-conventional' actuation mode. Here we offer a brief view of materials that have already been processed and investigated which could potentially fit for the purpose.

The composite requires a pair of materials, of which one soft with low dielectric permittivity and another with a much higher dielectric permittivity. However, an increase in permittivity is usually achieved by mixing some filler material in a soft elastomer matrix which, in turn, also causes an increase in stiffness. The soft material is usually made from either silicon or acrylic. It is currently accepted that acrylic elastomer tends to be the preferred material for large-strain applications, as shown by Michel *et al.* [30]. Custom synthetic elastomers can also be used and in general these materials exhibit similar properties. Various researchers have categorized them showing that generally these soft materials have a relative dielectric permittivity ε_r whose value is in the range 2–10 and a shear modulus μ lying between 50 kPa and 1 MPa [31–33]. Overall, the material parameters used throughout the paper of $\mu = 100$ kPa and $\varepsilon = 4.68\,\varepsilon_0$ represent a good approximation for a generic acrylic elastomer to be adopted as a soft phase.

We also showed that in a simple laminate, specially with the traction-free boundary conditions, k_2 needs to be kept as low as possible for a realistic values of k_1 at the transition. For a rank-two composite this requirement is not relevant which makes the latter a much more viable arrangement to achieve the contraction actuation mode. When looking for a suitable stiff material, the threshold for the rank-two laminate is $k_1 \approx 40$.

Two strategies have been developed to improve the dielectric constant of elastomers. The first one is blending the elastomer material with a highly polarizable ceramic such as barium titanate [34], titanium dioxide [35] or calcium copper titanate [36]. This method does not seem to provide very high permittivities, with most of these materials displaying values of k_1 limited to five. The second method consists of improving the permittivity by addition of conductive fillers into the matrix, such as carbon nanotubes [37–39] and graphene sheets [40–42], to form conductive filler/polymer composites. These materials seem much more suitable for our goal,

with permittivity ratios reaching in principle hundred of times. Two examples can be cited: Tian *et al.* [41] have proposed a graphene-filled material such that the computed ratios are $k_1 = 400$ and $k_2 = 65$; George *et al.* [38] synthesized a carbon nanotube composite that, coupled with the soft matrix, reaches the values of $k_1 = 170$ and $k_2 = 12$. Both of these materials would be suitable in a rank-two laminate to display the contraction mode, with the former also able to allow inversion of actuation when arranged as a simple laminate layout.

6. Conclusion

A method to improve the actuation performance of dielectric elastomer membrane is to create a composite material in which a phase with a high-dielectric permittivity is embedded in a soft elastomeric matrix. An efficient way to achieve the goal is to arrange the internal microstructure as a hierarchical laminate. In this paper we show that for small-strain electro-elasticity in plane strain a new, 'non-conventional' actuation mode consisting of longitudinal *contraction* could be available for laminates whose electromechanical and geometrical parameters assume values beyond some thresholds.

The first part of the investigation is devoted to simple laminates. For this class of composite we have studied two types of boundary conditions: 'aligned loading' and traction-free. For the former, the threshold for the permittivity ratios is approximately 50 and is almost independent of the contrast in shear modulus. For the latter, said threshold depends almost linearly on the contrast in mechanical stiffness. For both, the ideal grade of laminae with respect to the longitudinal direction is approximately 30°. The former boundary condition clearly highlights that the change in actuation mechanism with respect to the conventional elongation mode is due to the change in the strains that each phase undergoes to allow compatibility of the macroscopic deformation.

For a rank-two layout the number of variables involved to define the microstructure is higher and this proved to be advantageous for the optimization of the microstructure in order to limit the contrast in permittivity to achieve the new actuation mode. We have shown that the optimum configuration is able to ensure the minimum threshold for the whole range of the stiffness ratio.

As far as actuation strains are concerned, the maximization of contraction once one has verified the possibility of achieving the new mode must be conducted carefully as the outcome may vary greatly being very sensible to small changes of the quantities involved. In general, however, a rank-two composite outperforms a simple laminate at same volume fractions of the constituents.

The proposed research can be extended, on the one hand, by encompassing nonlinear electro-elastic effects, on the other hand, by adapting the framework to different types of active composite, e.g. magneto-elastic laminates [43–46].

Data accessibility. This article has no additional data.

Authors' contributions. P.L.: conceptualization, investigation, methodology, writing—original draft; M.G.: conceptualization, methodology, supervision, writing—original draft, writing—review and editing.

All authors gave final approval for publication and agreed to be held accountable for the work performed therein.

Conflict of interest declaration. We declare we have no competing interests.

Funding. This work was funded by the UK Engineering and Physical Sciences Research Council (EPSRC) grant no. EP/R513003/1.

Acknowledgements. P.L. acknowledges the support by the UK Engineering and Physical Sciences Research Council (EPSRC) grant no. EP/R513003/1 for the Cardiff University Centre for Doctoral Training. Work done under the auspices of GNFM (Gruppo Nazionale per la Fisica Matematica) of the Italian institute INDAM (Istituto Nazionale di Alta Matematica Francesco Severi).

Appendix A

Here we provide a method to solve the rank-two laminate, equation (4.5), following and adjusting that proposed by Tian [26]. The main problem to be tackled when solving equation (4.5) is that

of the explicit determination of $\mathbb{C}^{\mathrm{av}-1}$ and the average elastic concentration tensor $\mathbb{G}$ for the core; with the proposed approach, the latter is calculated implicitly. The jump conditions and the average quantities, equations (2.3) and (2.4), are used together with the governing equation (4.1) to obtain the following relationships:

$$\left.\begin{aligned} & c^a \boldsymbol{e}^a + c^b \boldsymbol{e}^b = \boldsymbol{e}^{\mathrm{av}}, \quad \boldsymbol{m}^0 \cdot (\boldsymbol{e}^a - \boldsymbol{e}^b)\boldsymbol{m}^0 = 0 \\ \text{and} \quad & (\mathbb{C}^a \boldsymbol{e}^a + \mathbb{A}^a \boldsymbol{E}^a \otimes \boldsymbol{E}^a - \mathbb{C}^b \boldsymbol{e}^b - \mathbb{A}^b \boldsymbol{E}^b \otimes \boldsymbol{E}^b)\boldsymbol{n}^0 = \boldsymbol{0}. \end{aligned}\right\} \tag{A 1}$$

Plugging the first of these into the last two gives

$$\left.\begin{aligned} & \boldsymbol{m}^0 \cdot \boldsymbol{e}^a \boldsymbol{m}^0 = \boldsymbol{m}^0 \cdot \boldsymbol{e}^{\mathrm{av}} \boldsymbol{m}^0 \\ \text{and} \quad & (c^a \mathbb{C}^b + c^b \mathbb{C}^a)\boldsymbol{e}^a \boldsymbol{n}^0 = \mathbb{C}^a \boldsymbol{e}^{\mathrm{av}} \boldsymbol{n}^0 - c^a [\mathbb{A}^a (\boldsymbol{g}^a \boldsymbol{E}^{\mathrm{av}} \otimes \boldsymbol{g}^a \boldsymbol{E}^{\mathrm{av}}) - \mathbb{A}^b (\boldsymbol{g}^b \boldsymbol{E}^{\mathrm{av}} \otimes \boldsymbol{g}^b \boldsymbol{E}^{\mathrm{av}})]\boldsymbol{n}^0. \end{aligned}\right\} \tag{A 2}$$

From any 2×2 matrix ψ, a column vector $\hat{\psi}$ can be defined as

$$\hat{\psi} = \begin{bmatrix} \psi_{11} \\ \psi_{22} \\ \frac{1}{\sqrt{2}}(\psi_{12} + \psi_{21}) \end{bmatrix}. \tag{A 3}$$

A fourth-order tensor can also be turned into a 2×2 matrix with matrices becoming a column vector. As an example, the elastic constitutive relations can be written as

$$\begin{bmatrix} S_{11} \\ S_{22} \\ \sqrt{2}\, S_{12} \end{bmatrix} = \begin{bmatrix} C_{1111} & C_{1122} & \sqrt{2}\, C_{1112} \\ C_{2211} & C_{2222} & \sqrt{2}\, C_{2212} \\ \sqrt{2}\, C_{1211} & \sqrt{2}\, C_{1222} & 2\, C_{1212} \end{bmatrix} \begin{bmatrix} e_{11} \\ e_{22} \\ \sqrt{2}\, e_{12} \end{bmatrix}. \tag{A 4}$$

Using this notation, T is defined as the column vector generated from the matrix $m_i^0 m_j^0$. For the goal, the following matrices need also to be defined, i.e.

$$\left.\begin{aligned} & L^{(i)}_{mn} = A^b_{ijkl} g^b_{km} g^b_{ln} n_j - A^a_{ijkl} g^a_{km} g^a_{ln} n_j, \\ & N^{(i)}_{kl} = (c^b C^a_{ijkl} + c^a C^b_{ijkl}) n_j \\ \text{and} \quad & O^{(i)}_{kl} = C^b_{ijkl} n_j, \end{aligned}\right\} \tag{A 5}$$

which come from the various components of equation $(\mathrm{A}\,2)_2$. Next, the following (3×3) matrices are constructed using the row vector forms of the newly defined matrices $L^{(i)}$, $N^{(i)}$ and $O^{(i)}$, as follows:

$$P = \begin{bmatrix} \hat{0}^T \\ c^b \hat{L}^{(1)T} \\ c^b \hat{L}^{(2)T} \end{bmatrix}, \quad R = \begin{bmatrix} T^T \\ \hat{N}^{(1)T} \\ \hat{N}^{(2)T} \end{bmatrix}, \quad Q = \begin{bmatrix} T^T \\ \hat{O}^{(1)T} \\ \hat{O}^{(2)T} \end{bmatrix}, \tag{A 6}$$

where $\hat{0}$ is a three-component null vector. equation $(\mathrm{A}\,2)_2$ can now be rewritten using the constructed matrices in a simpler manner, i.e.

$$R\hat{e}^a = Q\hat{e}^{\mathrm{av}} + P\tilde{E}, \tag{A 7}$$

where $\tilde{E}$ is the column vector of the matrix $E^{\mathrm{av}}_i E^{\mathrm{av}}_j$. Solving for e gives

$$\hat{e}^a = R^{-1} Q \hat{e}^{\mathrm{av}} + R^{-1} P \tilde{E}. \tag{A 8}$$

W is next defined as the matrix form of the fourth-order tensor

$$c^a A^a_{ijkl} g^a_{km} g^a_{ln} + c^b A^b_{ijkl} g^b_{km} g^b_{ln}, \tag{A 9}$$

which is then used with the constructed quantities to obtain an expression of the average total stress (equation $(4.1)_2$) as

$$\begin{aligned}\hat{S}^{\mathrm{av}} &= c^a\hat{S}^a + c^b\hat{S}^b = c^a\hat{C}^a\hat{e}^a + c^b\hat{C}^b\hat{e}^b + W\tilde{E}\\ &= [\hat{C}^b + c^a(\hat{C}^a - \hat{C}^b)R^{-1}Q]\hat{e}^{\mathrm{av}} + [c^a(\hat{C}^a - \hat{C}^b)R^{-1}P + W]\tilde{E}.\end{aligned} \tag{A 10}$$

As previously shown, the total stress is made up of two uncoupled terms, the mechanical term and the electrical one. By inspection, we can thus see that the effective coupling and elastic tensors for the composite can be obtained using the new available algebraic variables as follows:

$$\hat{C}^{\mathrm{av}} = \hat{C}^b + c^a(\hat{C}^a - \hat{C}^b)R^{-1}Q \quad \text{and} \quad \hat{A}^{\mathrm{av}} = c^a(\hat{C}^a - \hat{C}^b)R^{-1}P + W. \tag{A 11}$$

These moduli can now be used in the expression

$$\hat{e}^{\mathrm{av}} = \hat{C}^{\mathrm{av}^{-1}}\hat{A}^{\mathrm{av}}\tilde{E}, \tag{A 12}$$

to obtain the average strain. From (A 11) it is trivial now to obtain the inverse of $\hat{C}^{\mathrm{av}}$ and the use of the modulus $\mathbb{G}$, which was previously used to calculate $\mathbb{A}^{\mathrm{av}}$, has been incorporated implicitly in the procedure.

References

1. Pelrine R, Kornbluh RD, Joseph J. 1998 Electrostriction of polymer dielectrics with compliant electrodes as a means of actuation. *Sens. Actuators A: Phys.* **64**, 77–85. (doi:10.1016/S0924-4247(97)01657-9)
2. Kofod G, Wirges W, Paajanen M, Bauer S. 2007 Energy minimization for self-organized structure formation and actuation. *Appl. Phys. Lett.* **90**, 081916. (doi:10.1063/1.2695785)
3. Anderson IA, Gisby TA, McKay TG, O'Brien BM, Calius EP. 2012 Multi-functional dielectric elastomer artificial muscles for soft and smart machines. *J. Appl. Phys.* **112**, 041101. (doi:10.1063/1.4740023)
4. Calabrese L, Berardo A, De Rossi D, Gei M, Pugno NM, Fantoni G. 2019 A soft robot structure with limbless resonant, stick and slip locomotion. *Smart Mater. Struct.* **28**, 104005. (doi:10.1088/1361-665X/ab3de1)
5. Chiang C, Lin CK, Ju M. 2007 An implantable capacitive pressure sensor for biomedical applications. *Sens. Actuators A: Phys.* **134**, 382–388. (doi:10.1016/j.sna.2006.06.007)
6. Carpi F, Frediani G, Gerboni C, Germignani J, De Rossi D. 2014 Enabling variable-stiffness hand rehabilitation orthoses with dielectric elastomer transducers. *Med. Eng. Phys.* **36**, 205–211. (doi:10.1016/j.medengphy.2013.10.015)
7. Calabrese L, Frediani G, Gei M, De Rossi D, Carpi F. 2018 Active compression bandage made of dielectric elastomers. *IEEE ASME Trans. Mechatron.* **23**, 2328–2337. (doi:10.1109/TMECH.2018.2860789)
8. Chiba S, Waki M, Kornbluh R, Pelrine R. 2011 Current status and future prospects of power generators using dielectric elastomer. *Smart Mater. Struct.* **20**, 124006. (doi:10.1088/0964-1726/20/12/124006)
9. Bortot E, Denzer R, Menzel A, Gei M. 2014 Analysis of a viscous soft dielectric elastomer generator operating in an electric circuit. *Int. J. Solids Struct.* **78–79**, 205–215. (doi:10.1016/j.ijsolstr.2015.06.004)
10. Moretti G, Rosati Papini GP, Daniele L, Forehand D, Ingram D, Vertechy R, Fontana M. 2019 Modelling and testing of a wave energy converter based on dielectric elastomer generators. *Proc. R. Soc. A* **475**, 20180566. (doi:10.1098/rspa.2018.0566)
11. Lu T, Ma C, Wang T. 2020 Mechanics of dielectric elastomer structures: a review. *Extreme Mech. Lett.* **38**, 100752. (doi:10.1016/j.eml.2020.100752)
12. Siboni MN, Ponte Castañeda P. 2014 Fiber-constrained, dielectric-elastomer composites: finite-strain response and stability analysis. *J. Mech. Phys. Solids* **68** 211–238. (doi:10.1016/j.jmps.2014.03.008)
13. Lopez-Pamies O. 2014, Elastic dielectric composites: theory and application to particle-filled ideal dielectrics, *J. Mech. Phys. Solids*, **64**, 61–82. (doi:10.1016/j.jmps.2013.10.016)

14. Lefevre V, Lopez-Pamies O. 2017 Nonlinear electroelastic deformations of dielectric elastomer composites: I–Ideal elastic dielectrics. *J. Mech. Phys. Solids* **99**, 409–437. (doi:10.1016/j.jmps.2016.07.004)
15. deBotton G, Tevet-Deree L, Socolsky EA. 2007 Electroactive heterogeneous polymers: analysis and applications to laminated composites. *Mech. Adv. Mat. Struct.* **14**, 13–22. (doi:10.1080/15376490600864372)
16. Tian L, Tevet-Deree L, Bhattacharya K. 2012 Dielectric elastomer composites. *J. Mech. Phys. Solids* **60**, 181–198. (doi:10.1016/j.jmps.2011.08.005)
17. Gei M, Springhetti R, Bortot E. 2013 Performance of soft dielectric laminated composites. *Smart Mater. Struct.* **22**, 104014. (doi:10.1088/0964-1726/22/10/104014)
18. Rudykh S, Lewinstein A, Uner G. 2013 Analysis of microstructural induced enhancement of electromechanical coupling in soft dielectrics. *Appl. Phys. Lett.* **102**, 151905. (doi:10.1063/1.4801775)
19. Spinelli AS, Lopez-Pamies O. 2015 Some simple explicit results for the elastic dielectric properties and stability of layered composites. *Int. J. Eng. Sci.* **88**, 15–28. (doi:10.1016/j.ijengsci.2014.01.005)
20. Gei M, Mutasa KCK. 2018 Optimisation of hierarchical dielectric elastomer laminated composites. *Int. J. Non Linear Mech.* **103**, 266–273. (doi:10.1016/j.ijnonlinmec.2018.06.005)
21. Marín F, Martínez-Frutos J, Ortigosa R, Gil AJ. 2021 A convex multi-variable based computational framework for multilayered electro-active polymers. *Comput. Methods Appl. Mech. Eng.* **374**, 113567. (doi:10.1016/j.cma.2020.113567)
22. Bardella L, Volpini V, Gei M. 2022 On the effect of the volumetric deformation in soft dielectric composites with high phase contrast. *J. Elast.* **148**, 167–198. (doi:10.1007/s10659-022-09891-7)
23. Huang R, Suo Z. 2012 Electromechanical phase transition in dielectric elastomers. *Proc. R. Soc. A* **468**, 1014–1040. (doi:10.1098/rspa.2011.0452)
24. Springhetti R, Bortot E. 2014 Optimal energy-harvesting cycles for load-driven dielectric generators in plane strain. *IMA J. Appl. Math.* **79**, 929–946. (doi:10.1093/imamat/hxu025)
25. McMeeking RM, Landis CM. 2005 Electrostatic forces and stored energy for deformable dielectric materials. *J. Appl. Mech.* **72**, 581–590. (doi:10.1115/1.1940661)
26. Tian L. 2007 Effective behavior of dielectric elastomer composites. PhD thesis, California Institute of Technology.
27. Tevet-Deree L. 2008 Electroactive polymer composites - analysis and simulation. Ph.D. thesis, Ben-Gurion University.
28. Rudykh S. 2011 Stability of anisotropic electroactive polymers with application to layered media. *Z. Angew. Math. Phys.* **62**, 1131–1142. (doi:10.1007/s00033-011-0136-1)
29. Volpini V, Bardella L, Gei M. 2019 A note on the solution of the electro-elastic boundary-value problem for rank-two laminates at finite strains. *Meccanica* **54**, 1971–1982. (doi:10.1007/s11012-019-00974-9)
30. Michel S, Zhang X, Wissler M, Löwe C, Kovacs G. 2009 A comparison between silicone and acrylic elastomers as dielectric materials in electroactive polymer actuators. *Polym. Int.* **59**, 391–399. (doi:10.1002/pi.2751)
31. Jung K, Lee J, Cho M, Koo JC, Nam J, Lee Y, Choi HR. 2007 Development of enhanced synthetic elastomer for energy-efficient polymer actuators. *Smart Mater. Struct.* **16**, S288. (doi:10.1088/0964-1726/16/2/S13)
32. Romasanta LJ, Lopez-Manchado MA, Verdejo R. 2015 Increasing the performance of dielectric elastomer actuators: a review from the materials perspective. *Prog. Polym. Sci.* **51**, 188–211. (doi:10.1016/j.progpolymsci.2015.08.002)
33. Lau G-K, Ren Z-X, Chiang K-T. 2022 Effect of stretch limit change on hyperelastic dielectric actuation of styrene–ethylene/butylene–styrene (SEBS) copolymer organogels. *Smart Mater. Struct.* **31**, 095019. (doi:10.1088/1361-665X/ac7f0b)
34. Kumar A, Ahmad D, Patra K, Hossain M. 2021 Enhancement of electromechanical properties of natural rubber by adding barium titanate filler: an electro–mechanical study. *J. Appl. Polym. Sci.* **138**, 50991. (doi:10.1002/app.50991)
35. Liu H, Zhang L, Yang D, Yu Y, Yao L, Tian M. 2013 Mechanical, dielectric, and actuated strain of silicone elastomer filled with various types of TiO_2. *Soft Mater.* **11**, 363–370. (doi:10.1080/1539445X.2012.661821)
36. Zhang YY, Wang GL, Zhang J, Ding KH, Wang ZF, Zhang M. 2017 Preparation and properties of core–shell structured calcium copper titanate@polyaniline/silicone dielectric elastomer actuators. *Polym. Compos.* **40**, E62–E68. (doi:10.1002/pc.24479)

37. Kim J-Y, Kim T, Suk JW, Chou H, Jang J-H, Lee JH, Kholmanov IN, Akinwande D, Ruoff RS. 2014 Enhanced dielectric performance in polymer composite films with carbon nanotube-reduced graphene oxide hybrid filler. *Small* **10**, 3405–3411. (doi:10.1002/smll.201400363)
38. George N, Chandra CSJ, Mathiazhagan A, Joseph R. 2015 High performance natural rubber composites with conductive segregated network of multiwalled carbon nanotubes. *Compos. Sci. Technol.* **116**, 33–40. (doi:10.1016/j.compscitech.2015.05.008)
39. Xu Z, Zheng S, Wu X, Liu Z, Bao R, Yang W, Yang M. 2019 High actuated performance MWCNT/Ecoflex dielectric elastomer actuators based on layer-by-layer structure. *Compos. A: Appl. Sci. Manuf.* **125**, 105527. (doi:10.1016/j.compositesa.2019.105527)
40. Panahi-Sarmad M, Zahiri B, Noroozi M. 2019 Graphene-based composite for dielectric elastomer actuator: a comprehensive review. *Sens. Actuators A* **293**, 222–241. (doi:10.1016/j.sna.2019.05.003)
41. Tian M, Zhang J, Zhang L, Liu S, Zan X, Nishi T, Ning N. 2014 Graphene encapsulated rubber latex composites with high dielectric constant, low dielectric loss and low percolation threshold. *J. Colloid Interface Sci.* **430**, 249–256. (doi:10.1016/j.jcis.2014.05.034)
42. Ning N, Ma Q, Liu S, Tian M, Zhang L, Nishi T. 2015 Tailoring dielectric and actuated properties of elastomer composites by bioinspired poly(dopamine) encapsulated graphene oxide. *ACS Appl. Mater. Interfaces* **7**, 10 755–10 762. (doi:10.1021/acsami.5b00808)
43. Dorfmann A, Ogden RW. 2003 Magnetoelastic modelling of elastomers. *Eur. J. Mech. A/Solids* **22**, 497–507. (doi:10.1016/S0997-7538(03)00067-6)
44. Mohammadi NK, Galich PI, Krushynska AO, Rudykh S. 2019 Soft magnetoactive laminates: large deformations, transverse elastic waves and band gaps tunability by a magnetic field. *J. Appl. Mech.* **86**, 4044497. (doi:10.1115/1.4044497)
45. Rambausek M, Danas K. 2021 Bifurcation of magnetorheological film–substrate elastomers subjected to biaxial pre-compression and transverse magnetic fields. *Int. J. Non-Linear Mech.* **128**, 103608. (doi:10.1016/j.ijnonlinmec.2020.103608)
46. Polukhov E, Keip M-A. 2021 Multiscale stability analysis of periodic magnetorheological elastomers. *Mech. Mat.* **159**, 103699. (doi:10.1016/j.mechmat.2020.103699)